

# Light amplification in silicon nanocrystals by pump and probe transmission measurements

L. Dal Negro,<sup>a)</sup> M. Cazzanelli, B. Danese, and L. Pavesi

*INFN and Dipartimento di Fisica, Università di Trento, via Sommarive 14, 38050 Povo (Trento), Italy*

F. Iacona

*CNR-IMM, Sezione di Catania, I-95121 Catania, Italy*

G. Franzò and F. Priolo

*INFN and Dipartimento di Fisica, Università di Catania, I-95129 Catania, Italy*

(Received 9 April 2004; accepted 6 August 2004)

Net optical gain in silicon nanocrystals (Si-nc) has been measured by pump and probe transmission experiments. Si-nc active layers have been produced by plasma enhanced chemical vapor deposition on transparent quartz substrates. Continuous and pulsed pump and probe transmission measurements have shown clear evidences of net probe amplification with fast (nanosecond) response time. Transfer matrix and rate equations modeling of the nonlinear signal transmission allowed to extract the gain spectra for different pump intensities yielding good qualitative agreement with the experimental data. Gain cross sections per nanocrystals of the order of  $3 \times 10^{-16} \text{ cm}^2$  have been deduced. The physical origin of the optical amplification is interpreted within a four level recombination model describing the dynamics of strongly localized excitons at the Si-nc/SiO<sub>2</sub> interface. © 2004 American Institute of Physics. [DOI: 10.1063/1.1803613]

## I. INTRODUCTION

Since the early demonstration of room temperature photoluminescence in low-dimensional silicon nanostructures,<sup>1</sup> a variety of fabrication techniques have been used to produce silicon nanocrystals (Si-nc) with different sizes and size distributions allowing for widely tuneable emission bands. Although quantum confinement of carriers within the Si-nc is supposed to play a major role in increasing both the luminescence yield and the Si-nc emission energies, the exact nature of the radiative recombination mechanism still remains an open issue.<sup>1</sup> It is not clear whether emission is due to phonon assisted recombination of quantum confined excitons in Si-nc<sup>2,3</sup> or to radiative recombination of localized carriers at the Si-nc/SiO<sub>2</sub> interface.<sup>4</sup> In particular, many theoretical as well as experimental works<sup>4-11</sup> have suggested that oxygen-related centers and the geometrical relaxation of excited Si-nc can play a key role in the light emission process. More strikingly, optical gain in Si-nc has been demonstrated recently by several groups,<sup>12,13</sup> stimulating an exciting debate on its strengths and origin.

At present, optical gain has been observed in Si-nc samples prepared by different techniques: Si ion implantation,<sup>12,14</sup> plasma enhanced chemical vapor deposition (PECVD),<sup>9-11</sup> chemical deposition of amorphous silicon/silica superlattices,<sup>15</sup> electron beam deposition of SiO<sub>x</sub> films,<sup>16</sup> colloidal synthesis of silicon particles,<sup>17</sup> sol-gel dispersion of porous silicon fragments.<sup>18</sup> Optical gain has been measured in Si-nc rich waveguides by looking at the nonlinear increase of the amplified spontaneous emission

(ASE) with the excitation volume.<sup>19</sup> ASE is characterized by a fast (nanosecond time scale) time dynamics with an intensity threshold to superlinear behavior.<sup>8,10,15,20</sup> In addition, probe signal amplification in pump and probe transmission experiments under high pumping excitation conditions has been observed<sup>12</sup> and laser oscillations with spatially coherent speckle patterns in Si-nc light emission have been reported.<sup>17</sup>

Among all the different experimental approaches, important information can be achieved by time resolved experiments of the ASE signal from Si-nc waveguide. In addition to the usual slow emission decay peculiar of Si-nc (microseconds range), an intense ASE fast emission (nanoseconds time scale) appears either by increasing the pump fluence or by increasing the excitation volume.<sup>8-11,15</sup> ASE occurrence is the consequence of a delicate balance between Auger nonradiative recombinations and stimulated emission recombinations: whenever the Si-nc stimulated emission lifetime is shorter than the Auger lifetime optical gain can occur in Si-nc. Moreover, stimulated emission lifetime shortens as the Si-nc density increases and it critically depends on the pumping conditions.<sup>8-11</sup> Thus, materials properties as well as geometrical waveguide factors affect both the strength and the possibility of optical gain. Indeed, some Si-nc samples do not show optical gain in ASE studies<sup>21</sup> or in pump/probe waveguide studies.<sup>22</sup> This shows that the phenomenon is not completely understood and that the material itself has still to be optimized. Indications suggest that the gain is related to localized state recombinations either in the form of Si-Si dimers<sup>17</sup> or in the form of Si=O bonds formed at the interface between the Si-nc and the oxide<sup>23</sup> or within the oxide matrix.<sup>24</sup> The model introduced in Refs. 7, 9, and 11 relies on a four level recombination scheme where a large lattice relaxation in photoexcited small Si-nc gives rise to localized energy levels within the fundamental Si-nc band gap.

<sup>a)</sup>Present address: Materials Processing Center, Department of Materials Science and Engineering, Massachusetts Institute of Technology, Building 13, Room 41-34, 77 Massachusetts Avenue, Cambridge, MA 02139.

TABLE I. Total atomic Si content (obtained from Rutherford backscattering experiments measurements), temperatures of thermal treatment  $T_A$ , Si-nc concentration  $\xi$ , Si-nc radius estimated from transmission electron microscopy measurements, photoluminescence PL maxima ( $\lambda_m$ ), absorption coefficient at 400 nm ( $\alpha_0$ ), and modal gain  $g$  measured in ASE experiments [Ref. 10] at a wavelength of 750 nm.

Name	Si content (at. %)	$T_A$ (°C)	Si-nc (at. %)	$\xi$ (cm <sup>-3</sup> )	$\langle r \rangle$ (nm)	$\lambda_m$ (nm)	$\alpha_0$ ( $\times 10^3$ cm <sup>-1</sup> )	$g$ (cm <sup>-1</sup> )
A	42	1250	13	$6.30 \times 10^{18}$	1.7	906	9.1	48
B	39	1250	8.5	$8.33 \times 10^{18}$	1.5	795	4.1	-40

Further indications of optical gain are reported here by studying the nonlinear transmission of Si-nc samples. The transmission of a weak probe beam resonant to the stimulated emission transitions is measured as a function of the intensity of a strong pump beam with a short wavelength. Increase of the transmitted probe beam intensity with respect to the intensity of the beam in air reveals the occurrence of net optical gain. Since the continuous wave (CW) pump beam used here is usually very intense (some kW/cm<sup>2</sup>), the effect of additional thermal nonlinearities (thermal lensing, self-diffraction, etc.) is carefully considered. In particular, the response time of the nonlinear transmission shows that the transmission changes occur on a nanosecond timescale. The observation of fast transmission changes allows us to neglect the effects of thermally related experimental artifacts. We will address some of these important issues in the Appendix.

## II. EXPERIMENT

We studied Si-nc samples produced by high temperature annealing of substoichiometric silicon oxide (SiO<sub>x</sub>) thin films grown by PECVD on a quartz substrate. The structural and luminescence properties of these systems have been fully discussed elsewhere.<sup>9</sup> We focus here on two representative samples characterized by different total Si content: a sample obtained by deposition of 42 at. % of Si named sample A, and a sample obtained by deposition of 39 at. % of Si, named sample B. More detailed characteristics of these samples are listed in Table I. In both samples, the layer containing the Si-nc was 250 nm thick and it was embedded between two 100 nm thick deposited SiO<sub>2</sub> layers in order to form a slab waveguide structure. The ASE data collected on these two samples have been already reported in Ref. 9 and 11. Sample A shows gain while sample B does not. This is attributed to the delicate interplay between Auger recombinations and stimulated emission that prevents population inversion in sample B. Indeed sample B has a lower refractive index than sample A which is indicative of a lower packing density of Si-nc in sample B than in sample A.

In this experimental study, we investigate the nonlinear transmission of a weak probe beam as a function of the pump beam intensity, according to different excitation conditions. Figure 1 shows the geometry common to all our experiments, where normal incidence of the probe beam was used (to avoid pump-power dependent beam steering effects) while the pump beam was incident with an angle on the

sample surface. A video camera imaged the surface of the sample to check the relative positions of the pump and probe spots.

For CW experiments, the probe beam was supplied by the monochromatized emission of a short-arc air-cooled 1000 W Xe lamp whose intensity stability was carefully monitored. Spatial filtering of the probe light by two small pinholes allows a clean focusing of the probe beam on the sample surface to a 100  $\mu$ m diameter spot. No difference in the experimental results was observed as a function of the spectral width of the probe beam. We also used an HeNe laser line (632.8 nm) in some experiments. The probe beam, whose intensity on the sample surface was smaller than some  $\mu$ W (power density lower than few mW/cm<sup>2</sup>), was normally incident on the sample surface. In some experiments, the transmitted probe beam was imaged onto the entrance slit of a double spectrometer and detected using photon-counting technique. In others, when the probe beam was tightly monochromatized or when the HeNe laser was used, the transmitted probe beam was imaged onto a large area silicon photodetector connected with a digital oscilloscope triggered by a fast photodiode. Signal averaging was needed in this last case, degrading the time response of the system to  $\approx$ 1 ms. Spatial filtering was used on the collection line to reduce the luminescence signal from the sample excited by the high intensity of the pump beam. When the probe beam was switched off, a measure of the luminescence signal could be done. We performed experiments using as a pump beam the 457 nm or the 365 nm lines of an UV-extended Ar laser, focused at about 45° onto the sample surface which results in an ellipsoidal shaped spot of 200  $\times$  100  $\mu$ m<sup>2</sup>. The pump beam was chopped at about 24 Hz.

For pulsed excitation experiments, we used as probe beam an He-Ne laser (632.8 nm) or a CW diode laser (780 nm) and we excite the sample with a pulsed pump laser

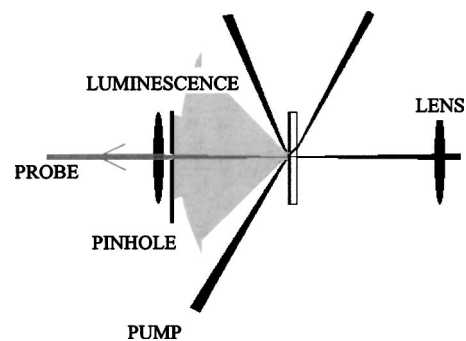


FIG. 1. Sketch of the pump and probe geometry used.

beam (355 nm). The pump beam was provided by the third harmonic of a Nd:yttrium aluminum garnet (YAG) laser whose repetition frequency was 10 Hz and pulse duration was 6 ns. Its intensity was varied by using a polarizing cube which prevented any displacement of the spot on the sample surface as it can occur with neutral density filters. We emphasize here that this strategy allowed us to maintain a very good alignment of the two beams regardless of the pumping intensity used. A camera continuously monitors the relative alignment of the pump and probe beam in all CW and pulsed experiments. The transmitted probe beam intensity was recorded by using a spectrometer and an ultrafast (10 ps time resolution) Hamamatsu streak camera used in photon-counting mode. Spectral filtering of the sample luminescence turns out to be crucial when performing experiments at high pulse fluence since the sample emission can significantly affect the experimental results. Lenses were used to focus the probe beam on a spot size (1 mm) smaller than the spot size of the pump beam on the sample (1 cm wide). Care was used to keep the pump beam fluence lower than the damage threshold of the sample.

### III. DATA ANALYSIS

As the pump beam is pulsed or chopped, we recorded the transmitted intensity under three different pumping conditions.

(1) Sample photoexcited (pump beam on the sample) but no probe beam on the sample, which allows to measure the luminescence and the noise signal at the wavelength of the probe beam, named  $I_{PL}$ .

(2) Both the pump and the probe beam on the sample, which allows to measure the transmitted probe beam intensity when the sample *is* photoexcited, named  $I_{ON}$ .

(3) No pump beam on the sample but the probe beam on the sample, which allows to measure the transmitted probe beam intensity when the sample *is not* photoexcited, named  $I_{OFF}$ .

Let us define  $T_{OFF} = I_{OFF}/I_0$  and  $T_{ON} = I_{ON} - I_{PL}/I_0$ , where  $I_0$  is the incident probe beam intensity. Then the transmission enhancement caused by the photoexcitation is  $T_{sample} = T_{ON}/T_{OFF} = I_{ON} - I_{PL}/I_{OFF}$ .

In a very simple modeling, if we use the Beer's law then

$$I_{OFF} = I_0 \exp[-(\alpha_{QZ}d_{QZ} + \alpha_{Si-nc}(J_P = 0)d_{Si-nc})], \quad (1)$$

where  $\alpha_{QZ}$  ( $d_{QZ}$ ) is the absorption coefficient (thickness) of both the quartz and the SiO<sub>2</sub> layers, and  $\alpha_{Si-nc}$  ( $d_{Si-nc}$ ) the power dependent absorption coefficient (thickness) of the Si-nc layer, when the pump power density  $J_P$  is zero. If we assume that the effect of photoexcitation is simply to change the properties of the Si-nc, then

$$I_{ON} - I_{PL} = I_0 \exp[-[\alpha_{QZ}d_{QZ} + \alpha_{Si-nc}(J_P)d_{Si-nc}]]. \quad (2)$$

By dividing these two expressions we get that

$$\begin{aligned} T_{sample} &= \exp[-\alpha_{Si-nc}(J_P) + \alpha_{Si-nc}(J_P = 0)] \\ &= \exp(-\Delta\alpha_{Si-nc}d_{Si-nc}) \approx 1 - \Delta\alpha_{Si-nc}d_{Si-nc} \\ &= 1 + gd_{Si-nc}, \end{aligned} \quad (3)$$

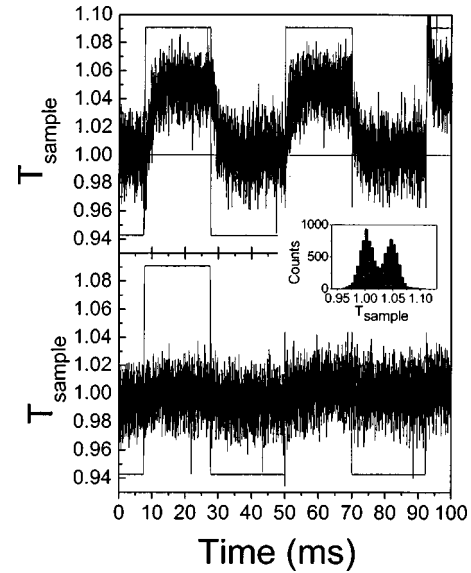


FIG. 2.  $T_{sample}$  (straight line) of sample A pumped by a 457 nm laser pump and temporal profile of the pump laser beam (dark line): (top panel) 2 kW/cm<sup>2</sup> pump intensity (bottom panel) 50 W/cm<sup>2</sup> pump intensity. The probe beam was provided by an He-Ne laser at 632.8 nm. The inset shows the histogram of  $T_{sample}$  for the top panel.

where  $g$  is the Si-nc gain coefficient.  $T_{sample}$  is related to the differential absorption  $\Delta\alpha_{Si-nc}$  of the Si-nc. This holds only when it is assumed that the pump beam has no effect on the transmission properties of the quartz and SiO<sub>2</sub> layers. The last equality in Eq. (3) is verified whenever other nonlinear effects, such as saturation of optical transitions, absorption bleaching, optical stark effects, etc., are negligible. In this case and if  $T_{sample} > 1$  we have a direct evidence of probe beam amplification due to optical gain ( $g > 0$ ). On the other hand if we measure  $T_{ON} > 1$  we have a direct measure of probe beam amplification with respect to the overall losses in the structure.

### IV. CONTINUOUS WAVE EXCITATION RESULTS

Figure 2 shows the time profile of  $T_{sample}$  of the CW probe beam (provided by a He-Ne laser at 632.8 nm) in presence of a chopped CW pump beam for low (bottom panel) and high (top panel) pumping power density as measured by a large area Si photodetector (sensible element size 1 cm<sup>2</sup>). The detector was positioned close ( $\sim 2$  cm) to the sample without any optical elements in between in order to avoid heat induced geometrical probe beam distortions and thermal lensing effects on the probe beam (see Appendix). Apart from a noisy weak modulation, no influence on the probe transmission is observed at low pumping power (see Fig. 2 bottom). On the contrary, at high pump power density, a strong modulation of the transmitted signal is observed which follows the on-off modulation of the pump beam. A statistical analysis of the data shows that the increase of  $T_{sample}$  is significant as it is larger than one standard deviation of the data (see inset in Fig. 2). The limited response time of the apparatus (large area photodiode and electronics) causes the initial transient. The same time constant is also observed when the luminescence signal alone is recorded. However, after the initial transient (1 ms) the transmitted intensity sig-

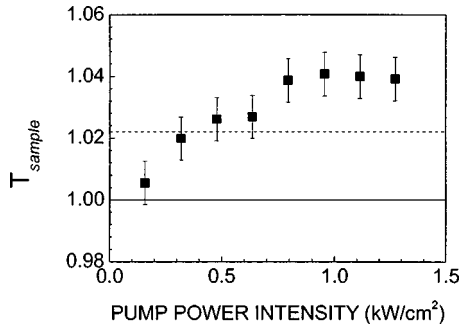


FIG. 3.  $T_{\text{sample}}$  (sample A) as a function of the pump power density for a probe beam wavelength of 750 nm and pump beam wavelength of 365 nm. The dashed horizontal line is the transparency threshold with respect to the probe beam in air.

nal is constant excluding major heating problems or damaging of the sample. On these basis we attributed the transmission enhancement to probe beam amplification.

Figure 3 shows the pump power density  $J_p$  dependence of  $T_{\text{sample}}$  at a wavelength of 750 nm. The monochromatized emission of the Xe lamp provided the probe beam. Time averaging of the signal allowed to achieve a typical standard deviations of 0.007 in  $T_{\text{sample}}$  (error bars in Fig. 3). If we use Eq. (3) with the assumption that  $-\Delta\alpha_{\text{Si-nc}}=g$ , then  $T_{\text{sample}} - 1/d_{\text{Si-nc}} \approx g \approx N_{\text{Si-nc}}\sigma \Rightarrow \sigma \approx T_{\text{sample}} - 1/d_{\text{Si-nc}} N_{\text{Si-nc}}$ , where  $\sigma$  is the Si-nc gain cross section. Increasing  $J_p$  the gain increases, at a critical  $J_p \approx 0.5 \text{ kW/cm}^2$  transparency is reached where the gain equals to the losses in the substrate and above it single pass net gain is observed. The gain values turn out to be a linearly increasing function of  $J_p$  up to a value of about  $1600 \pm 300 \text{ cm}^{-1}$  ( $\sigma_g \approx 3 \times 10^{-16} \text{ cm}^{-2}$ ). For  $J_p \geq 1 \text{ kW/cm}^2$ , gain saturation is observed.

Figure 4 shows the spectral dependence of  $T_{\text{OFF}}$  and  $T_{\text{ON}}$ . In these measurements, the probe beam was provided by the broad band emission of a Xe lamp and a synchronous detection of  $T_{\text{ON}}$  and  $T_{\text{OFF}}$  was made possible by using two detection chains. It should be noted that  $T_{\text{ON}}$  and  $T_{\text{OFF}}$  are normalized with respect to the intensity of the probe beam incident on the sample which was measured by the same apparatus in absence of the sample.  $T_{\text{OFF}}$  does not depend on  $J_p$  (Fig. 4, top panel).  $T_{\text{OFF}}$  shows clear interference fringes which are caused by the multilayered structure of the sample.  $T_{\text{ON}}$  shows the same interference fringes (no dramatic heating effect on the real part of refractive indices). In addition, in a region centered at about 700 and 100 nm wide,  $T_{\text{ON}}$  increases significantly with increasing  $J_p$  and reaches the transparency threshold ( $T_{\text{ON}}=1$ ) at about  $0.5 \text{ kW/cm}^2$ . Note that the interference fringes structure is not affected by the pump power, i.e., the maxima and minima do not shift with  $J_p$ . For even greater  $J_p$ ,  $T_{\text{ON}}$  is larger than 1. In this region the probe beam is amplified with respect to its value before the sample, i.e., the sample shows high values of the optical gain which compensates even for the losses caused by probe beam propagation in the quartz substrate. No similar effect is observed in a reference quartz substrate without Si-nc. Other samples show either an increase in the transmitted intensity up to the transparency or no influence of the pump beam (sample B). On the  $T_{\text{ON}}$  curve for the maximum  $J_p$  used we added the standard deviation of the data as error bars to

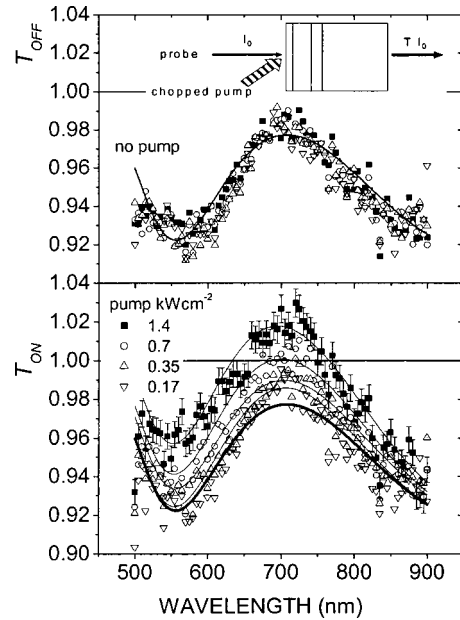


FIG. 4. Transmission spectra (points) for increasing pumping power densities integrated during the time interval when the pump beam is on (bottom panel) or is off (top panel). The various pump powers and the relative symbols are given as legend in the graph. The lines are simulation of the experimental data for the various power densities. The thick line in the bottom panel is the no pump results of the simulation of top panel. (Inset) Sketch of the experiment and of the sample structure. Sample A was used.

emphasize that the increase of  $T_{\text{ON}}$  is in excess of the measurement errors. Note also that  $T_{\text{OFF}}$  is measured synchronously with  $T_{\text{ON}}$  the pump beam is chopped and  $T_{\text{ON}}$  and  $T_{\text{OFF}}$  are measured during the time the pump is present or absent on the sample. The multiple symbols for  $T_{\text{OFF}}$  in the figure refers to the various  $J_p$  used to measure  $T_{\text{ON}}$ . The spread of the  $T_{\text{OFF}}$  data is less than the power induced increase of  $T_{\text{ON}}$  for the largest  $J_p$  used.

To extract the gain spectra, a transfer matrix calculations of the transmission through the sample has been performed. The experimental data of  $T_{\text{OFF}}$  were simulated by considering the sample formed by four optical layers (see inset in Fig. 4) characterized by a thickness of 270, 117 nm, 500.13  $\mu\text{m}$  and a refractive index of 1.98, 1.50, 1.35 for the Si-nc layer, the silica cladding layers and the quartz substrate, respectively.  $T_{\text{ON}}$  was simulated with the same parameters except that a wavelength dependent positive imaginary part in the refractive index  $\mathbf{n}$  was used for the Si-nc layer, where  $\mathbf{n}=n+i\kappa$  and  $\kappa=1/4\pi g(\lambda)\lambda$ .  $g(\lambda)$  was the only free function in the simulation and was described by a gaussian profile. Quite good simulations of the  $T_{\text{ON}}$  data for the various  $J_p$  have been achieved (see lines in Fig. 4 bottom panel). The resulting gain spectra for the various  $J_p$  are shown in Fig. 5. As  $J_p$  increases, both the peak and the width of the gain spectrum increase, a weak blueshift is also observed. By comparing the gain spectra with the luminescence spectra, a very large blueshift in the gain is observed. Figure 6 compares the gain spectrum at high  $J_p$  measured in this work with the spectral dependence of the fast component of the ASE measured by time-resolved variable stripe length measurements in Refs. 9–11. Despite the very different experimental methods and the different pumping conditions, the

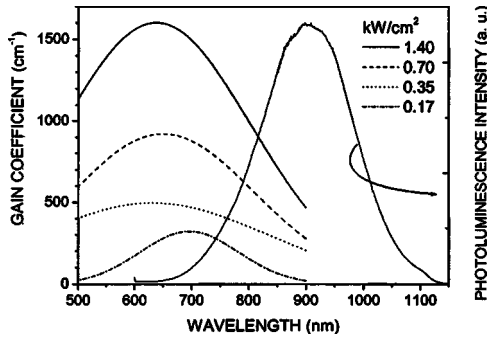


FIG. 5. Gain coefficient spectra used in the transfer matrix modeling of the transmission data of Fig. 4 for various pump power densities. The spectrum on the right is the luminescence spectrum of the sample measured at low pump power.

two spectra show remarkable similarities indicating that the physical origin of the gain as measured by pump-probe experiments and of the stimulated emission observed in luminescence experiments are the same.

**V. PULSED EXCITATION**

In the preceding section we have shown several evidences of single pass amplification in Si-nc systems. However, the measurements had a 1 ms time resolution due to experimental constraints. To investigate the response time of the nonlinear transmission change due to optical amplification we performed a time resolved experiment where we measured the transmitted intensity of a CW probe beam (at 632.8 or 780 nm) when the sample was excited by a pulsed pump beam. Figure 7 reports the time dependence of  $I_{ON}$ ,  $I_{OFF}$ , and  $I_{PL}$  for sample A under a high excitation fluence  $\Phi$ . The bottom panel refers to a probe beam of 633 nm where the luminescence is weak and the top panel refers to a probe beam of 780 nm where the luminescence intensity is high. In Fig. 7,  $I_{OFF}$  and  $I_{ON}$  coincides except when the sample is excited with the short pump pulse. In coincidence with the arrival of the pump pulse on the sample,  $I_{ON}$  increases for few nanoseconds and then decreases. The time dynamics of

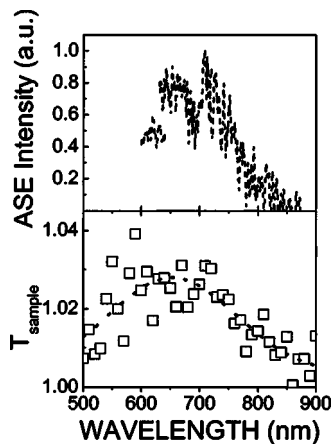


FIG. 6. (bottom panel) Spectral dependence of  $T_{sample}$  for sample A. Pump wavelength 365 nm and intensity 1.5 kW/cm<sup>2</sup>. Dotted line is the result of the transfer matrix model. (Top panel) Spectral dependence of the amplified stimulated emission (ASE) measured on sample A on a time integration window of 100 ns. The pumping fluence is 200 mJ/cm<sup>2</sup>. After Ref. 8.

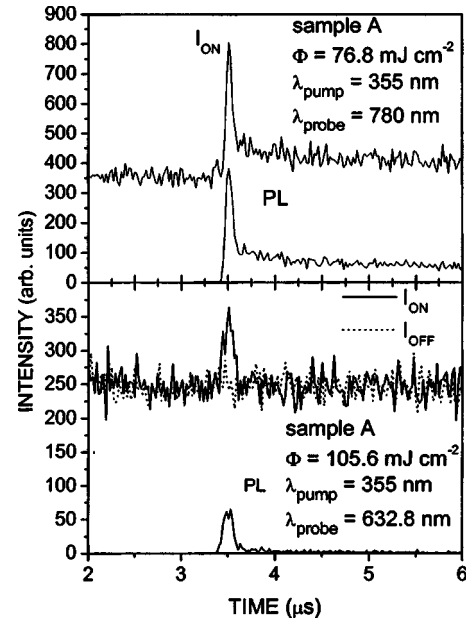


FIG. 7. Time dependence of the transmitted probe beam intensity in pulsed photoexcitation conditions. The line is the transmitted intensity when the pulsed pump laser was present. The dotted line is the transmitted intensity without the pulsed pump laser. The line labeled PL is the signal measured when the pump beam was exciting the sample but no probe beam was present. Sample is sample A. The probe wavelength is 623.8 nm for the bottom panel and 780 nm for the top panel.

$I_{ON}$  reflects the time dynamics of the fast component of the luminescence observed in Si-nc,<sup>10</sup> which is reflected in the time dependence of  $I_{PL}$  shown as the weak signal in Fig. 7. Note that the time profiles were recorded with exactly the same experimental parameters except for the presence/absence of the probe beam signal. Quite interesting the time profiles of the signal measured when the pulsed excitation was present and when the pulse excitation was absent are coincident apart for the time when the sample is photoexcited. This means that no significant heating or damaging of the sample occurs in the experiments. The top panel refers to the data at 780 nm: at this wavelength the luminescence is very strong and is characterized by a two component decays, one fast due to ASE and one slow due to exciton recombinations.<sup>10</sup>

In order to test whether a transmission enhancement is observed, the peak intensity of  $I_{ON}$  and  $I_{PL}$  are used to compute  $T_{sample}$ . Since we recorded the data using photon counting techniques, the intensity counts are distributed according to a Poisson distribution and, hence, the errors on the intensity  $I$  is equal to  $\sqrt{I}$ .<sup>25</sup> For a probe wavelength  $\lambda_{probe} = 632.8$  nm  $I_{ON}$  increases by  $114 \pm 35$  counts when the pump beam is exciting the sample while the peak intensity of  $I_{PL}$  reaches a maximum value of only  $65 \pm 8$  counts. That is  $I_{ON}$  under the pulsed excitation increases more than the contribution to  $I_{ON}$  due to the photoluminescence signal. This is a clear evidence of probe beam amplification and the lifetime of this effect exactly coincides with the one observed in the fast PL as a result of optical amplification. The same applies for  $\lambda_{probe} = 780$  nm. Here  $I_{ON}$  increases by  $449 \pm 47$  counts while  $I_{PL} = 382 \pm 19$  counts on the maximum.

We repeated the measurements on sample B which does

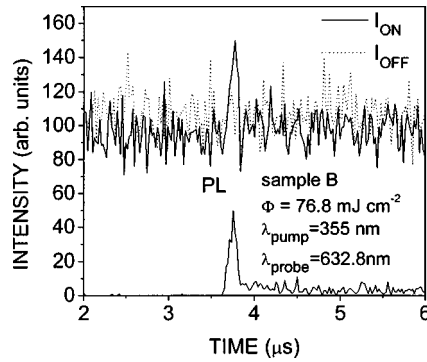


FIG. 8. Time dependence of the transmitted probe beam intensity in pulsed photoexcitation conditions for sample *B* and a probe wavelength of 632.8 nm.

not show optical gain in time-resolved variable stripe length measurements.<sup>9</sup> Figure 8 reports the time dependence of  $I_{ON}$ ,  $I_{OFF}$  and  $I_{PL}$  for sample *B* for high  $\Phi$ .  $I_{ON}$  increases when the sample is excited, but the increase is only due to the luminescence of the sample. No  $T_{\text{sample}} > 1$  is observed.

## VI. RATE EQUATION MODELING

We have already proposed<sup>7,9,11</sup> a full set of rate equation for a phenomenological description of optical gain in Si-nc. Our model considered the interplay of nonradiative Auger recombinations within a four level system (Fig. 9) whose microscopic nature is currently under debate. Here we simply aim to discuss a nonlinear transmission model based on the integration of the four level population rate equations. The direct observation of nonlinear probe beam amplification allow us to neglect the Auger contributions in a first approximation.

The set of steady state rate equations in our simplified model is given by

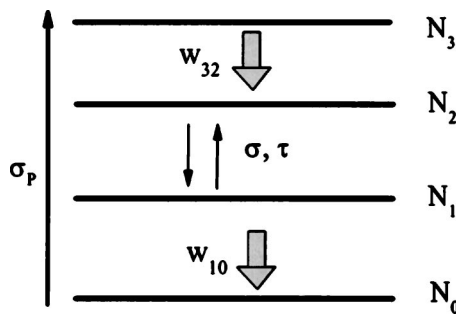


FIG. 9. Sketch of the four level recombination system used for the nonlinear transmission calculations.

$$\frac{dN_0}{dt} = -\sigma_p \phi_p N_0 + w_{10} N_1 = 0,$$

$$\frac{dN_1}{dt} = \sigma \phi N_2 - \sigma \phi N_1 + \frac{N_2}{\tau} - w_{10} N_1 = 0,$$

$$\frac{dN_2}{dt} = w_{32} N_3 - \sigma \phi N_2 + \sigma \phi N_1 - \frac{N_2}{\tau} = 0,$$

$$\frac{dN_3}{dt} = \sigma_p \phi_p N_0 - w_{32} N_3 = 0,$$

$$\sum_i N_i = N_{\text{tot}}, \quad (4)$$

where  $N_i$  represent the level population densities ( $i = 0, \dots, 3$ , Fig. 9) which sum up to  $N_{\text{tot}}$  the active center density in the system,  $\sigma_p$  is the absorption cross section at the pump wavelength,  $\phi_p$  is the pumping photon flux,  $w_{ij}$  are the relaxation rates from the  $i$  to the  $j$  energy levels,  $\phi$  is the probe beam photon flux, and  $\tau$  is the total lifetime of the emitting level  $N_2$ . The positive small-signal gain cross section  $\sigma$  allows for probe beam amplification.

After some algebraic manipulations on the system (4), it can be demonstrated that the population inversion term can be simply expressed as

$$N_2 - N_1 = \frac{N_{\text{tot}}}{\left(1 + \frac{w_{10} + \sigma \phi}{\sigma \phi + 1/\tau} + \frac{w_{10}}{w_{32}} + \frac{w_{10}}{\sigma_p \phi_p}\right)} \left(\frac{w_{10} - 1/\tau}{\sigma \phi + 1/\tau}\right). \quad (5)$$

On the other hand, the propagation equation for the probe beam photon flux  $\phi$  is

$$\frac{\partial \phi}{\partial z} = -(N_1 - N_2) \sigma \phi. \quad (6)$$

The integration of the propagation Eq. (6) can be performed analytically once the population difference  $N_1 - N_2$  has been computed. Note that the population inversion term depends on the probe beam photon flux density via Eq. (5) which accounts for gain saturation effects. Let us define for a sample  $d$  long, the transmission as  $T = \phi_{\text{out}} / \phi_{\text{in}}$ , where  $\phi_{\text{in}}$  and  $\phi_{\text{out}}$  are the incident ( $z=0$ ) and transmitted ( $z=d$ ) probe photon flux, respectively. After some computations we can achieve a quite simple implicit expression relating the pump beam photon flux  $\phi_p$  with the system transmission  $T$

$$\phi_p = \frac{\frac{w_{10} w_{32}}{\sigma_p} \left( \sigma \phi_{\text{in}} (1 - T) - \frac{\ln(T)}{\tau} \right)}{w_{32} \ln(T_0) \left( w_{10} - \frac{1}{\tau} \right) + \phi_{\text{in}} (T - 1) (2w_{32} \sigma + w_{10} \sigma) + \left( \frac{w_{10}}{\tau} + \frac{w_{32}}{\tau} + w_{32} w_{10} \right) \ln(T)}, \quad (7)$$

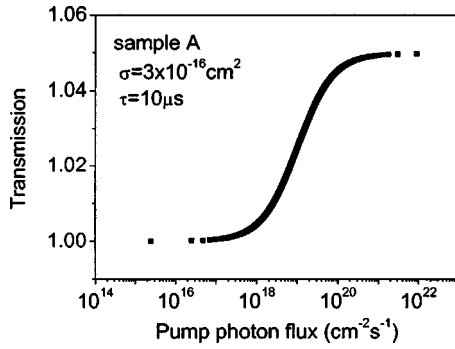


FIG. 10. Numerical simulation of the nonlinear probe transmission in a four level system as a function of the incident radiation photon flux. The simulation parameters are:  $w_{10}=w_{32}=10^{15} \text{ s}^{-1}$ ,  $\sigma_p=10^{-14} \text{ cm}^2$ ,  $\sigma=3 \times 10^{-16} \text{ cm}^2$ ,  $\tau=10 \text{ }\mu\text{s}$ ,  $\phi_{in}=10^{10} \text{ cm}^{-2} \text{ s}^{-1}$ ,  $d=270 \text{ nm}$ ,  $N_{tot}=6 \times 10^{18} \text{ cm}^{-3}$ .

where  $T_o=\exp(-\sigma N_{tot}d)$ . Figure 10 reports  $T$  versus  $\phi_p$  for a set of Si-nc parameters reported in the figure caption. We notice that since the effect of propagation losses and reflection is not included, the model yields transparency (transmission equal to one) at low pump values, while increasing  $\phi_p$  the transmission grows nonlinearly because of stimulated emission up to saturation.

Figure 11 shows a qualitative comparison between the model and the experimental data for sample A. A similar trend with a nonlinear growth of transmission up to a 4% when  $\phi_p$  is increased over three orders of magnitude is observed, even though the pump photon flux involved in the simulations are smaller than the experimental ones. This could be due to the simple assumptions of neglecting the optical losses and of assuming an ideal pumping efficiency. Also other nonradiative recombination paths should be included in the model to get a better quantitative agreements. However, our aim here was to show that a simple nonlinear transmission model based on a set of rate equations can qualitatively describe the experimental findings. This reinforces the overall physical interpretation of the experimental results which is based on similar results obtained via ASE studies.<sup>9-11</sup>

**VII. CONCLUSIONS**

Net optical amplification of a probe beam through a Si-nc sample has been measured with different experimental

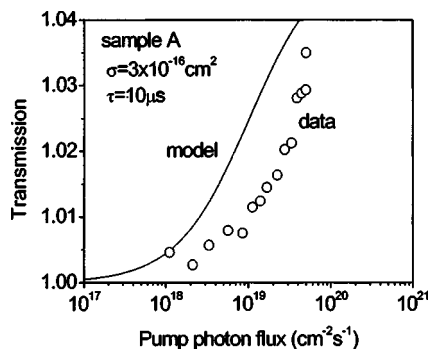


FIG. 11. Numerical simulation of the four level transmission enhancement (line) with the same parameters as in Fig. 10 and measured probe beam transmission enhancement (disks) as a function of the pump photon flux for sample A and probe beam wavelength of 750 nm.

set-ups. Gain cross section per nanocrystal similar to the one measured in Ref. 12 on ion implanted samples or estimated in Ref. 10 for PECVD samples are deduced by these measurements. Note that larger material gain is reported in Ref. 12 than in this work, possibly due to a larger Si-nc density in the ion implanted samples. However it is clear that more work is needed to understand the role on the gain of the various material parameters. A fast (nanoseconds time scale) response time of the nonlinear transmission has been measured in agreement with the occurrence of a fast emission component under high fluence pulsed excitation in ASE experiments. The optical amplification spectra have been extracted from pump and probe data showing a close similarity with the stimulated emission spectra measured by time resolved ASE analysis. The qualitative behavior of the nonlinear transmission measured here supports a four level recombination model for the occurrence of optical gain, even though a microscopic understanding of the gain effect is still under debate.

**ACKNOWLEDGMENTS**

We acknowledge the financial support of INFN through the RAMSES project, of EC through the SINERGIA project and of MIUR through FIRB projects. S. Ossicini and N. Daldosso are thanked for helpful discussions, C. Ot3n for helping in transfer matrix simulations with gain and Z. Gaburro for helpful suggestions concerning the experimental setups.

**APPENDIX: HEATING EFFECTS**

Thermal heating of highly photoexcited samples (especially when the pump is CW) can lead to experimental artifacts in pump and probe experiments. In this appendix we try to estimate the role of thermal nonlinearities in our measurements.

**1. Thermal nonlinearity response time**

The physical origin of thermal nonlinearities consists in the refractive index change of an excited material as a results of direct photon absorption. Thermal processes can usually lead to large nonlinear optical effects. However, the time scale for the refractive index change is usually longer than the scale of electronic phenomena, leading to strongly time dependent nonlinear optical effects. Assuming that  $\Delta T$  is the laser induced temperature change in the material, we can assume that  $\Delta T$  obeys a heat-transport equation:<sup>26</sup>

$$C_v \frac{\partial \Delta T}{\partial t} - \kappa \nabla^2 \Delta T = \alpha P, \tag{A1}$$

where  $C_v$  is the heat capacity per unit volume,  $\kappa$  is the thermal conductivity of the material,  $\alpha$  the absorption coefficient, and  $P$  is the pump power. Equation (A1) can be solved with the appropriate boundary conditions yielding the temperature change and the refractive index profile in any given physical situation.

However, the thermal response time  $\tau$  (the time taken for a temperature distribution to reach its new steady state after laser beam switching on or off) can be simply estimated by replacing the partial derivatives in Eq. (A1) with  $\partial\Delta T/\partial t \rightarrow \Delta T/\tau$  and  $\nabla^2\Delta T \rightarrow \Delta T/(w/2)^2$  where  $w$  is the pump beam waist on the sample surface. Equation (A1) can therefore be approximated by the simple relation:<sup>26</sup>

$$\tau \approx \frac{C_v(w/2)^2}{\kappa}. \quad (\text{A2})$$

We assume that the thermal conductivity of Si-nc samples is very close to that of fused SiO<sub>2</sub> because most the Si-nc are embedded in SiO<sub>2</sub>. Then,  $\kappa \approx 1.4$  W/mK and  $C_v = 1.67 \times 10^6$  J/m<sup>3</sup>. Considering that the pump beam spot size is  $w \approx 100$   $\mu\text{m}$ , we estimate  $\tau \approx 3$  ms. This time is the typical time for which thermal effects develop and play a role.

## 2. Heating induced absorption

$\Delta T$  can be calculated on the basis of a theoretical heat conduction model developed by Tang and Herman.<sup>27</sup> The model has been successfully applied to explain laser induced thermal effects in free standing porous silicon.<sup>28,29</sup> By using the formula given in Ref. 29 and the SiO<sub>2</sub> parameters for the Si-nc layer, we calculated a  $\Delta T$  of up to 1300 °C for high pump power density ( $\sim 1$  kW/cm<sup>2</sup>). This  $\Delta T$  must be considered a severe overestimate of the actual one since the Si-nc thermal conductivity is more likely bigger than the one of SiO<sub>2</sub>, the Si-nc layer is not free standing but deposited on a 0.5 mm thick quartz substrate and the thermal conductivity increases when the sample temperature raises. Indeed in free standing porous silicon a saturation of the temperature increase at values of about 700 °C has been observed at high pumping intensity.<sup>28</sup> However, these estimates point to an important role played by sample heating during CW experiments.

Heating is not only constricted to the photoexcited region but has a significant spatial extension. The spatial profile of  $\Delta T$  has been thoroughly studied in Ref. 30, which for our experimental conditions translates in an elliptic heated surface of  $400 \times 200$   $\mu\text{m}^2$  around the photoexcited region. Thus in the experiment we are faced with two regions: the photoexcited region, as large as the pump beam spot, and the heated region, twice as large. Figure 12 top panel reports a line scan of the probe beam spot position with respect to the pump beam spot position. When the two spots overlap  $T_{\text{sample}} > 1$  (crossed region); when the two spots are far apart  $T_{\text{sample}} \approx 1$  within the error bars of the measurements; when the two spots are shifted by 100–200  $\mu\text{m}$   $T_{\text{sample}} < 1$  (dashed region). In this last case, the probe is probing the heated region and thermally induced absorption is measured.<sup>28</sup> The bottom panels in Fig. 12 show the transmitted probe beam intensity versus time: the transmitted beam intensity increases (decreases) when the probe beam is aligned (misaligned) with respect to the pump beam. During the time intervals when the pump is off, the two temporal profiles are equal which indicates no permanent sample damage or average increase of the temperature of the sample. Figure 12 shows that when proper alignment between probe and pump

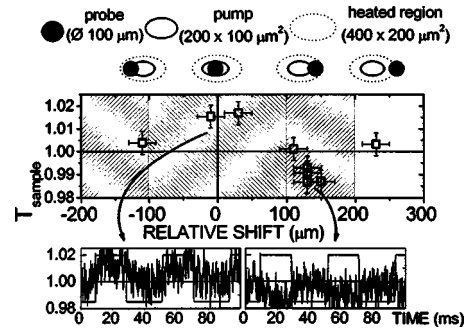


FIG. 12. (top panel)  $T_{\text{sample}}$  at 632.8 nm for various relative shifts of the pump and probe beams. Two zones are enlightened in the figure: the photoexcited zone and the heated region. In the top part, schematics are shown of the various regions considered in the analysis with their extensions and of the relative probe positions during the measurements. (bottom panel)  $T_{\text{sample}}$  as a function of time for two alignment conditions (left probe aligned with the pump, right probe misaligned with the pump) indicated by the arrows. The square wave shows the pump beam profile on the sample. (1.21 kW/cm<sup>2</sup> pump power density, 24 Hz chopper frequency). The time response of the detecting chain was limited by the need of signal averaging (trigger jitter) and by the slow silicon photodiode we used.

is achieved, optical gain can overcome the thermal induced absorption. The luminescence of the sample recorded under these pumping conditions does not evidence any of the significant effects (white emission, strong nonlinearity in intensity, etc.) reported in Ref. 29 and attributed to nonlinearity in the emission due to heating.

## 3. Thermal lensing effects

As we have seen in the previous sections, large temperature rises can be induced under strong pumping. Thus thermally induced nonlinearity in the refractive index of the nanocrystal material must be carefully considered. In particular, the phenomenon of thermal lensing could play a role in the relative alignment of the pump/probe beams and in the imaging of the transmitted beam on the detector. In the thermal lensing regime, a pump induced spatial profile of the refractive index is induced due to the local temperature rise. This can distort the optical path of a propagating probe beam in a way similar to a lens. A thermal focal length  $f_{\text{therm}}$  can be defined. It can be demonstrated<sup>31</sup> that

$$f_{\text{therm}} = 2\kappa\pi\left(\frac{w}{2}\right)^2\left[\frac{dn}{dT}P(1 - e^{-ad})\right]^{-1}, \quad (\text{A3})$$

where  $dn/dT$  is the temperature dependent change of the refractive index, which is  $\approx 6 \times 10^{-6}/\text{K}$  for fused quartz or silica.<sup>32</sup> Using this value, a pump power of 0.1 W (maximum pump power density of 1 kW/cm<sup>2</sup>) and a beam waist of 100  $\mu\text{m}$ , we got  $f_{\text{therm}} \approx 4$  cm. As this value is significantly longer than the active Si-nc layer thickness and even of the quartz substrate thickness, we can neglect effects due to thermal lensing in our experiment. The measurements reported in Fig. 2 confirm this conclusion.

<sup>1</sup>S. Ossicini, L. Pavesi, and F. Priolo, in *Light Emitting Silicon for Micro-photonics*, Springer Tracts in Modern Physics Vol. 194 (Springer, Berlin 2003).

<sup>2</sup>D. Kovalev, H. Heckler, G. Polisski, and F. Koch, *Phys. Status Solidi B* **215**, 871 (1999).

- <sup>3</sup>L. Khriachtchev, M. Räsänen, S. Novikov, O. Kilpelä, and J. Sinkkonen, *J. Appl. Phys.* **86**, 5601 (1999).
- <sup>4</sup>A. B. Filonov, S. Ossicini, F. Bassani, and F. Arnaud d'Avitaya, *Phys. Rev. B* **65**, 195317 (2002).
- <sup>5</sup>M. V. Wolkin, J. Jorne, P. M. Fauchet, G. Allan, and C. Delerue, *Phys. Rev. Lett.* **82**, 197 (1999).
- <sup>6</sup>M. Caldas, *Phys. Status Solidi B* **217**, 641 (2000).
- <sup>7</sup>S. Ossicini, C. Arcangeli, O. Bisi, E. Degoli, M. Luppi, R. Magri, L. Dal Negro, and L. Pavesi, in *Towards the First Silicon Laser*, NATO Advanced Studies Institute, Series 11, edited by L. Pavesi, S. Gaponenko, and L. Dal Negro (Kluwer Academic, Dordrecht, 2003), Vol. 93 p. 261.
- <sup>8</sup>L. Khriachtchev, S. Novikov, and J. Lahtinen, *J. Appl. Phys.* **92**, 5856 (2002).
- <sup>9</sup>L. Dal Negro *et al.*, *Physica E (Amsterdam)* **16**, 297 (2003).
- <sup>10</sup>L. Dal Negro, M. Cazzanelli, L. Pavesi, D. Pacifici, G. Franzò, F. Priolo, and F. Iacona, *Appl. Phys. Lett.* **82**, 4636 (2003).
- <sup>11</sup>L. Dal Negro *et al.*, in *Towards the First Silicon Laser*, NATO Advanced Studies Institute, Series 11, edited by L. Pavesi, S. Gaponenko, and L. Dal Negro (Kluwer Academic, Dordrecht, 2003), Vol. 93 p. 145.
- <sup>12</sup>L. Pavesi, L. Dal Negro, C. Mazzoleni, G. Franzò, and F. Priolo, *Nature (London)* **408**, 440 (2000).
- <sup>13</sup>*Towards the first silicon laser*, NATO Advanced Studies Institute, Series 11, edited by L. Pavesi, S. Gaponenko, and L. Dal Negro (Kluwer Academic, Dordrecht 2003), Vol. 93.
- <sup>14</sup>K. Luterova, I. Pelant, I. Mikulskas, R. Tomasiunas, D. Muller, J. J. Grob, J. L. Rehspringer, B. Hönerlage, *J. Appl. Phys.* **91**, 896 (2002); and unpublished.
- <sup>15</sup>J. Ruan, P. M. Fauchet, L. Dal Negro, M. Cazzanelli, and L. Pavesi, *Appl. Phys. Lett.* **83**, 5479 (2003).
- <sup>16</sup>L. Khriachtchev, M. Rasanen, S. Novikov, and J. Sinkkonen, *Appl. Phys. Lett.* **79**, 1249 (2001).
- <sup>17</sup>M. Nayfeh, S. Rao, N. Barry, A. Smith, and S. Chaieb, *Appl. Phys. Lett.* **80**, 121 (2002).
- <sup>18</sup>K. Luterová, K. Dohnalová, V. Švrček, I. Pelant, J.-P. Likforman, O. Crégut, P. Gilliot, and B. Hönerlage, *Appl. Phys. Lett.* **84**, 3280 (2004).
- <sup>19</sup>L. Dal Negro, P. Bettotti, M. Cazzanelli, L. Pavesi, D. Pacifici, *Opt. Commun.* **229**, 337 (2003).
- <sup>20</sup>K. Luterová, D. Navarro, M. Cazzanelli, T. Ostatnický, J. Valenta, S. Cheylan, I. Pelant, and L. Pavesi, (unpublished).
- <sup>21</sup>J. Valenta, I. Pelant, and J. Linnros, *Appl. Phys. Lett.* **81**, 1396 (2002).
- <sup>22</sup>R. G. Elliman, M. J. Lederer, N. Smith, B. Luther-Davies, *Nucl. Instrum. Methods Phys. Res. B* **206**, 427 (2003).
- <sup>23</sup>N. Daldosso *et al.*, *Phys. Rev. B* **68**, 085327 (2003).
- <sup>24</sup>L. Khriachtchev, M. Räsänen, S. Novikov, and L. Pavesi, *Appl. Phys. Lett.* **85**, 1511 (2004).
- <sup>25</sup>D. F. Walls and G. J. Milburn, *Quantum Optics* (Springer, Berlin 1994), p. 46.
- <sup>26</sup>W. Boyd, *Nonlinear Optics* (Academic, New York 2003).
- <sup>27</sup>H. Tang and I. P. Herman, *J. Vac. Sci. Technol. A* **8**, 1608 (1990).
- <sup>28</sup>H. Koyama and P. M. Fauchet, *Appl. Phys. Lett.* **73**, 3259 (1998).
- <sup>29</sup>H. Koyama and P. M. Fauchet, *J. Appl. Phys.* **87**, 1788 (2000).
- <sup>30</sup>M. Lax, *J. Appl. Phys.* **48**, 3819 (1977).
- <sup>31</sup>J. P. Gordon, R. C. C. Leite, R. S. Moore, S. P. S. Porto, and J. R. Whinnery, *J. Appl. Phys.* **36**, 3 (1965).
- <sup>32</sup>C. Yin, Y. Inatomi, N. I. Wakayama, and W. D. Huang, *Cryst. Res. Technol.* **38**, 785 (2003).